A magnetically separable SO$_4$/Fe-Al-TiO$_2$ solid acid catalyst for biodiesel production from waste cooking oil

Jabbar Gardy[a], Amin Osatiashtiani[b], Oscar Céspedes[c], Ali Hassanpour[a,*], Xiaojun Lai[a,*], Adam F. Lee[d], Karen Wilson[d], Mohammad Rehan[e]

[a] School of Chemical and Process Engineering, University of Leeds, West Yorkshire, Leeds, LS2 9JT, UK
[b] European Bioenergy Research Institute, Aston University, Aston Triangle, Birmingham, B4 7ET, UK
[c] School of Physics and Astronomy, University of Leeds, West Yorkshire, Leeds, LS2 9JT, UK
[d] School of Science, RMIT University, Melbourne, VIC3001, Australia
[e] Centre of Excellence in Environmental Studies (CEES), King Abdulaziz University, Jeddah, Saudi Arabia

ABSTRACT

A novel magnetic SO$_4$/Fe-Al-TiO$_2$ solid acid catalyst was synthesized for biodiesel production *via* the (trans) esterification of waste cooking oil (WCO). The nanocomposite catalyst was prepared by the sequential functionalisation of commercial rutile/anatase mixed phase TiO$_2$ nanoparticles (NPs) with alumina as a buffer layer, and subsequently hematite to impart magnetic character, prior to sulfation with chlorosulfonic acid to introduce Brønsted acidity. XRD showed that the SO$_4$/Fe-Al-TiO$_2$ catalyst comprised titania (rutile and anatase phases), aluminium sulphate, and hematite nanoparticles, while electron microscopy revealed the layer-by-layer assembly of these components within the SO$_4$/Fe-Al-TiO$_2$ catalyst. FTIR confirmed the presence of surface sulphate groups SO$_4^{2-}$ and S$_2$O$_7^{2-}$/S$_3$O$_{10}^{2-}$, creating a predominantly Brønsted acid catalyst with high acid loading. The catalyst achieved 96% fatty acid methyl ester (FAME) yield from WCO after 2.5 h of reaction at 90 °C, using 3 wt % of the magnetic catalyst, and a methanol:oil molar ratio of 10:1. SO$_4$/Fe-Al-TiO$_2$ was also effective for feedstocks containing up to 20 wt% of free fatty acid (FFA), and showed excellent stability for WCO (trans) esterification over 10 recycles.

1. Introduction

Developing alternative fuel has attracted a growing interest over the past twenty five years due to the depletion of fossil fuels, human health hazards and climate change [1,2]. Biodiesel, which comprises fatty acid alkyl esters (FAMEs) is gaining popularity as an alternative fuel because of its availability, being eco-friendly, non-toxicity and biodegradability [3,4]. Currently around 90% of the worldwide biodiesel in industry is being produced by homogenous acid/alkaline catalyzed (trans)esterification process of triglycerides in oleaginous food crops with methanol [5]. However, using these food oil crops would require significant amounts of freshwater and arable lands. This could also lead to food security problems in developing countries [6]. Waste(used) cooking oil [7], (micro)algae [8], and jatropha seeds [9] could be used as alternative non-food source feedstocks to overcome the aforementioned issue for the production of cheap biodiesel fuel. Nevertheless, such raw materials for biodiesel production contain a high level of free fatty acids (FFA) resulting in soap (fatty acid salts) formation [10]. Therefore, design of heterogeneous catalysts, as alternative to homogeneous

catalysts currently used in the industrial synthesis of biodiesel fuel, has been the subject of intensive research to overcome this problem [11].

Solid acid catalyst design has received considerable attention for biodiesel production from cheap and non-food feedstocks. This is because solid acid catalysts can simultaneously perform esterification of FFAs and transesterification of triglycerides without (1) soap formation, (2) corrosion of the reactors, (3) quenching steps, and (4) neutralisation of by-products. They also allow for process intensification *via* continuous biodiesel production [12]. More importantly, the potential recovery and reusability of these catalysts from the (trans)esterification reaction make them preferable for industrial biodiesel production [13–16]. Numerous synthetic routes are emerging for the preparation of solid acid catalysts for different applications [17–33]. Sulfated metal oxides have been recently used as typical solid acid catalysts for the (trans)esterification process and we have also recently reported the synthesis of a novel titanium sulphate oxide [Ti(SO$_4$)O] catalyst for the (trans)esterification of waste cooking oil (WCO) to form biodiesel [5]. The incorporation of sulphate groups into metal oxides mainly enhance the Brønsted acidity property and catalytic activity [34–36]. However,

low surface area and/or difficulty in the separation process of solid acid catalysts still persist main drawbacks [18,30,37–39]. Some researchers have reported that the presence of magnetic properties in catalysts increases their re-usability by enabling fast recovery with little loss using external magnetic fields [26,40–43]. Magnetic properties in solid acid catalysts are an excellent mean for separating the catalyst from the reaction media but the surface of magnetic oxide materials are unstable under acidic conditions, being very sensitive compared to titania, and the particles can be easily aggregated into large clusters due to anisotropic dipolar interactions, which result in loss of their catalytic activity [44,45]. Several methods have been introduced to overcome this issue, including a layer-by-layer coating of the surface with different metal oxides and polymers [28,30,39]. Therefore, it is necessary to develop a novel magnetic solid material as a potential catalyst candidate that could fulfil all requirements for the industrial (trans)esterification process. Here, we report, for the first time, the design and synthesis of a multifunctional magnetic solid acid [SO_4/Fe-Al-TiO_2] catalyst for the production of biodiesel from WCO. Characterisation and application investigations of this new designed magnetic solid acid catalyst for biodiesel production *via* (trans)esterification of WCO are carried out and reported.

2. Experimental

2.1. Materials

Aluminium iso-propoxide (+98% granular, Al(O-i-Pr)$_3$) was purchased from Alfa Aesar whilst oleic acid (≥99%), hydrochloric acid (37%, HCl) and chlorosulfonic acid (HSO$_3$Cl, 99%) were obtained from Fluka Analytical. Titanium (IV) oxide nanoparticles (99.5%, product number 718467-100G), methanol (≥99.9%), ethanol (≥99.8%), ethylene glycol (99.8%, EG), ammonium hydroxide (28–30 %, NH$_4$OH), ferric chloride hexahydrate (≥98%, FeCl$_3$.6H$_2$O), ferrous chloride tetrahydrate (≥99.99%, FeCl$_2$.4H$_2$O), (methyl heptadecanoate (≥99.5%), *n*-heptane (≥99%), acetone (99.9%) and *n*-hexane (99.5%) were purchased from Sigma–Aldrich. All chemicals were used without further purification. The sample of WCO was provided by a local restaurant in Leeds, and was used as the feedstock for biodiesel production. The collected WCO was pre-treated by filtration and then heated at 100 °C for 5 h to reduce the water content; the resulting WCO contained 0.14 wt% moisture and 2 wt% FFA.

2.2. Catalyst preparation

The catalyst was synthesised *via* stepwise deposition of alumina and iron oxides on to commercial TiO$_2$ NPs. This is expected to both increase the surface area, and introduce magnetic character, the former should minimise mass transfer limitations by providing a large pore network for subsequent liquid phase catalysis [46]. The addition of alumina and iron oxides into the commercial TiO$_2$ catalyst should also improve the thermal stability, acidity of TiO$_2$ catalyst as well as catalytic activity as compared to previously used Ti(SO$_4$)O [5] and sulphated Fe$_2$O$_3$/TiO$_2$ [47].

2.2.1. Synthesis of alumina coated TiO$_2$

0.1 mols of aluminium iso-propoxide was dispersed in a round-bottomed flask containing 50 ml of ethanol. Subsequently, 1 g of commercial TiO$_2$ NPs and 5 ml of ammonium hydroxide were added to the flask, and the resulting solution stirred at 250 rpm for 10 min. The resulting suspension was refluxed at 80 °C under vigorous stirring until a light yellowish gel formed. The solvent was then evaporated by ageing the solution without agitation at room temperature for 24 h, and the powder obtained then washed repeatedly with 1:1 vol% ethanol:deionised water. The aluminium impregnated TiO$_2$ was then oven-dried overnight at 100 °C, prior to static calcination in air at 400 °C for 5 h. This sample is denoted Al-TiO$_2$.

#### 2.2.2. Preparation of iron oxide coated Al-TiO$_2$

The preceding Al-TiO$_2$ material was subsequently iron oxide functionalised through the co-precipitation of Fe^{2+} and Fe^{3+} precursors under alkaline conditions (Fe^{2+} + 2 Fe^{3+} + 8 OH$^-$ → Fe$_3$O$_4$ + 4 H$_2$O [48,49]). 0.15 mols ferric chloride hexahydrate and 0.1 mols ferrous chloride tetrahydrate were separately dissolved in 50 ml of a 1:1 vol% ethanol:deionised water under ultrasonication until they formed clear solutions. The resulting solutions were both added dropwise to a three neck round-bottomed flask containing 2 g of Al-TiO$_2$ nanoparticles suspended in 50 ml of ethanol and 10 ml of ethylene glycol under stirring. 25 ml of concentrated ammonium hydroxide were injected into the reaction mixture until the pH reached 9–10. The reaction mixture was then heated to 75 °C under reflux and a N$_2$ atmosphere, and vigorously stirred for 2 h, followed by static ageing for 12 h. The gel obtained was separated using an external magnetic field, and rinsed repeatedly with 1:1 ethanol: deionised water until chloride ions could not be detected (using AgNO$_3$) in the washings. The resulting dark-reddish gel was then oven dried overnight at 80 °C, prior to calcination under static air at 400 °C for 4 h. This temperature chosen to be below the threshold to induce an anatase to rutile phase transition, [50] yet sufficient to form hematite. This sample is denoted Fe-Al-TiO$_2$.

2.2.3. Chlorosulfonic acid functionalization of Fe-Al-TiO$_2$

1 g of Fe-Al-TiO$_2$ was dispersed in 50 ml of dry toluene by ultrasonication. The suspension was then cooled to −5 °C using an ice bath, and gently stirred during the addition of 2 ml chlorosulfonic acid, injected at 0.1 ml min^{-1}. The suspension was refluxed at 60 °C for 2 h under a N$_2$ atmosphere, and the resulting solid magnetically separated from the solution, thoroughly washed with fresh toluene until neutral washings were obtained, and then oven-dried overnight prior to calcination at 400 °C for 4 h. This sample, representing the final solid acid catalyst is denoted SO$_4$/Fe-Al-TiO$_2$. The overall catalyst synthesis is summarised in Scheme 1.

2.3. Catalyst characterisation

Sample crystallinity was explored by powder X-ray diffraction (XRD) using a Bruker D8 diffractometer and Cu Kα radiation (1.54 Å, 40 kV/40 mA) between 10 and 70° and steps of 0.0495° (35 s per step). Fourier transform infrared (FTIR) spectra were recorded at room temperature using a Nicolet iS10 spectrometer between 650 and 4000 cm^{-1} with a resolution of 4 cm^{-1}. Catalyst morphology and particle size distributions were examined using a cold field emission scanning electron microscopy (CFE-SEM, SU8230 Hitachi) operated at 1–2 kV, and scanning transmission electron microscopy (STEM, FEI Titan Themis Cubed 300) operated at 300 kV. Samples were dispersed in acetone over a carbon-coated copper grid. Elemental compositions and spatial distributions were determined by HAADF detector in conjunction with an energy dispersive X-ray spectrometer (EDS, Oxford INCA 350). Nitrogen adsorption-desorption isotherms were measured on a Micromeritics TriStar 3000 porosimeter at 77 K, on samples degassed overnight at 120 °C in vacuo. Thermogravimetric analysis (TGA) was performed on a Mettler Toledo (TGA/DSC-1) stare system under N$_2$ gas at 50 ml min^{-1} and a heating rate of 10 °C min^{-1} from 25 to 900 °C. Brønsted/Lewis acid character was determined by diffuse reflectance IR spectroscopy (DRIFTS) on pyridine titrated samples. Prior to DRIFTS analysis, samples were diluted to 10 wt% in KBr, and pyridine adsorbed *ex-situ* by wetting samples with physisorbed pyridine removed in vacuo at 100 °C overnight. Spectra were collected at 50 °C on a Thermo Scientific Nicolet iS50 spectrometer using an environmental cell and Smart Collector accessory. Acid loadings were determined by TGA-MS through the thermal desorption of reactively formed propene, with samples first saturated with *n*-propylamine, and physisorbed *n*-propylamine removed in vacuo at 30 °C overnight. Analysis of untreated and *n*-propylamine treated samples was performed using a Mettler Toledo TGA/DSC-2 instrument connected *via* a heated capillary to a Pfeiffer
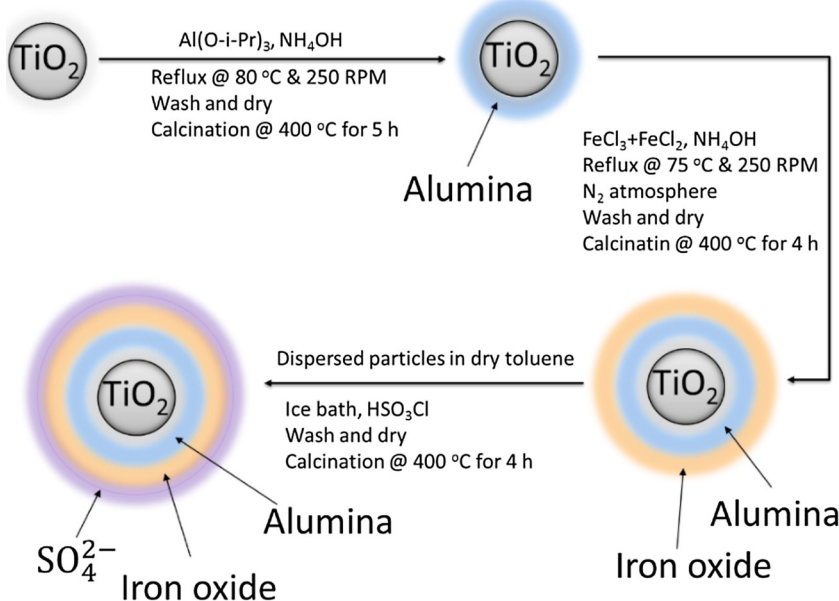
Scheme 1. Schematic of SO$_4$/Fe-Al-TiO$_2$ catalyst synthesis.

ThermoStar mass spectrometer under flowing He at 30 ml min^{-1} and a heating rate of 10 °C min^{-1} from 40 to 800 °C. The amount and temperature at which reactively-formed propene ($m/z = 41$) and ammonia ($m/z = 15$) were evolved are respectively quantitative measures of the number and strength of acid sites at which n-propylamine chemisorbed. Magnetic properties were assessed on a Maglab 9 T vibrating sample magnetometer (VSM, Oxford instruments) at room temperature. 10–15 mg of sample was accurately weighed into a gelatine capsule and loaded into the sample holder which was subsequently placed between pick-ups coils located in a He flow cryostat and sinusoidally vibrated. The centre of sample oscillation was first positioned at the vertical centre of the pick-up coils, and off-centre. The sample was held in a 2 Tesla magnetic field at room temperature, with the resulting change in magnetic flux induced within the coils and associated electromagnetic field (EMF) proportional to the magnetic moment (M) of the sample. Finally, the coercivity (H$_c$) and the remanence (M$_r$ in unit Am^2) were determined from the magnetic moment/ external magnetic field curve.

2.4. Catalyst test

The (trans)esterification of WCO was conducted in a glass batch reactor equipped with a temperature controller, mechanical stirrer, and a reflux condenser. Specific amounts of SO$_4$/Fe-Al-TiO$_2$ catalyst, methanol and pre-treated WCO were charged to the reactor at room temperature. The solid–liquid–liquid phases were mixed under constant stirring and heated to the required temperature. After a specified time, the reaction mixture was subsequently transferred to a separating funnel and allowed to cool to room temperature. The FAME-containing layer was then separated from the residuals by centrifugation at 9000 rpm for 10 min, and a few ml of the FAME then analysed by offline GC–MS (580S, Perkin Elmer Clarus gas chromatograph, equipped with a 560S mass spectrometer) according to the modified ASTM and EU standard methods [5].

2.5. Biodiesel characterisation

The flash point of the produced biodiesel was measured by an auto ramp, closed cup, flash point tester (Setaflash series 3). The temperature was ramped at 1–2 °C min^{-1} until the flash was captured. Biodiesel density at 15 °C was measured using the pycnometric method. A Bohlin-Gemini 150 rotary rheometer (Malvern, UK) was used to measure the

biodiesel viscosity. Trace moisture content was analysed by volumetric Karl Fischer titration (Mettler Toledo-V20, Germany). The acid values and FFA% of the oil and synthesised biodiesel were measured according to standard methods [51,52]. The acid value and the percentage of free fatty acid of biodiesel were calculated as follows:

$$\text{Acid value, mgKOH/g} = \frac{(V_{bs}-V_b)* C * 56.11}{W} \quad (1)$$

$$\text{Free fatty acid, } \% = \frac{(V_{bs}-V_b)* C * 28.246}{W} \quad (2)$$

Where: V$_{bs}$ is consumed volume of titrate for the biodiesel sample in ml; V$_b$ is consumed volume of titrate for the blank in ml; C is exact concentration of standardised alcoholic potassium hydroxide solution (mole/l) and W is mass of biodiesel sample used in g.

The biodiesel cloud point was determined using a differential scanning calorimetry (DSC 1, Mettler Toledo, UK) equipped with an intracooler system (Huber TC45): 5 ± 2.5 mg of biodiesel sample was weighted in a 40 µl sealed aluminium pan and placed in the DSC sample chamber and heated to 50 °C at 1 °C min^{-1} and held for 5 min to homogenise the sample should it contain any wax compounds. The system was then cooled to −30 °C at 1 °C min^{-1} and held for 5 min, with onset temperature of the initial exothermic peak during cooling defined as the cloud point [12]. The sample was maintained under flowing nitrogen at 50 ml min^{-1} throughout. Finally, the thermal stability of the biodiesel was assessed on a Stanton Redcroft thermogravimetric analyser (TGA-TGH 1000) on 20–25 mg of biodiesel sample which was heated from 25 to 600 °C at 10 °C min^{-1} under flowing air at 50 ml min^{-1}.

3. Results and discussion

3.1. Catalyst characterisation

3.1.1. Crystalline structure

The crystallinity of SO$_4$/Fe-Al-TiO$_2$ was explored through XRD, which revealed reflections characteristic of rhombohedral α-Fe$_2$O$_3$ (JCPDS-ICDD: 01-076-4579), rhombohedral aluminium sulphate (millosevichite, JCPDS-ICDD: 00-042-1428), and tetragonal titanium dioxide (anatase, JCPDS-ICDD: 04-006-9240 and rutile, JCPDS-ICDD: 01-076-9000) as shown in Fig. 1. The sharp reflections of α-Fe$_2$O$_3$ and
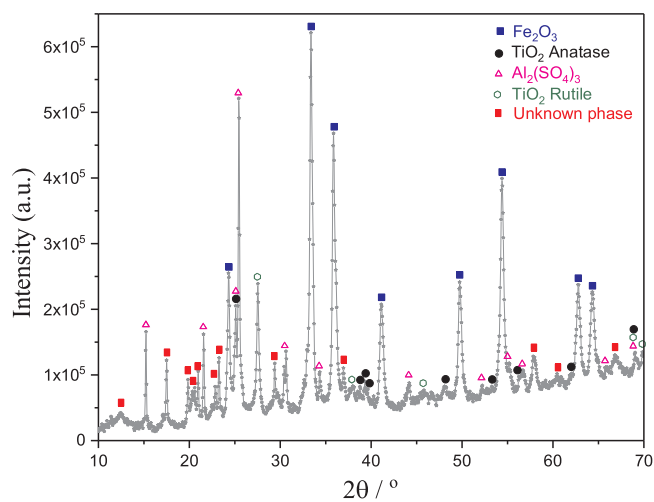
**Fig. 1.** Powder XRD pattern of SO$_4$/Fe-Al-TiO$_2$ catalyst.

Table 1
Crystallite sizes and *d*-spacings for components of SO$_4$/Fe-Al-TiO$_2$.

Phase	Reflection	2θ/°	FWHM/°	*d*-spacing/Å	Crystallite size/nm
Anatase	[101]	25.1	0.15	3.5	56
Rutile	[110]	27.5	0.19	3.2	42
α-Fe$_2$O$_3$	[104]	33.4	0.24	2.7	34
Al$_2$(SO$_4$)$_3$	[113]	25.4	0.15	3.5	56

aluminium sulfate evidence a highly ordered (extended) hematite phase, while those for titania were far weaker/broader consistent with small crystallites. Corresponding volume-averaged crystallite sizes and *d*-spacings for the most intense reflection of each phase are given in Table 1.

3.1.2. Electron microscopy

SEM of the initial aluminium functionalised titania reveals agglomerates of approximately 50 nm spherical particles (Supplementary document, Fig. S1). Corresponding TEM reveals tetragonal and

Table 2
EDS elemental analysis of Fe-Al-TiO$_2$.

Element	O	Ti	Al	Fe
wt%	36.9	32.6	16.5	14.0

hexagonal particles, some of which exhibit a core-shell like (Fig. S2a), with some evidence for anatase truncated octahedron crystallites terminating in [001]. The mean particle size was around 15–25 nm (Fig. S2b). HRTEM and EDX analysis (Fig. 2) is consistent with the formation of a low contrast amorphous alumina shell (Fig. S2a inset), approximately 3 nm thick, encapsulating a denser titania core.

SEM (Fig. S3) and TEM (Fig. S4) images of the Al-TiO$_2$ material after iron oxide functionalisation (Fe-Al-TiO$_2$) again reveal dense agglomerates of ~50 nm diameter and irregular shape nanoparticles, some of which are decorated with very small (< 10 nm) higher contrast nanoparticles which we attribute to hematite. Particle agglomeration may well reflect the magnetic character imparted by the iron oxide component. Elemental analysis (Table 2) of Fe-Al-TiO$_2$ reveals a near 1:1 Al:Ti atomic ratio (Fig. S5), and Fe:Al ratio of 0.4 consistent with only partial decoration of the surface of the alumina encapsulated titania nanoparticles. EDS elemental maps of Fe-Al-TiO$_2$ are shown in Fig. 3, demonstrate that Al and Fe are deposited as relatively homogenous shells around titania nanoparticles, illustrated in Fig. S6.

The sulfonated Fe-Al-TiO$_2$ was subsequently examined by SEM (Figs. S7–9) and TEM (Fig. 4). SEM micrographs reveal little change in the morphology upon sulfonation, with dense aggregates of irregular shaped nanoparticles around 50 nm diameter visible. Corresponding TEM confirm the presence of a range of nanoparticle shape and size (< 50 nm), with lattice fringes of 0.356 nm attributable to the rhombohedral millosevichite form of Al$_2$(SO$_4$)$_3$ (Fig. 4a), [110] planes of anatase (Fig. 4b), and [110] and [012] planes of rutile TiO$_2$ (Figs. 4c and e) and rhombohedral hematite (Fig. 4e). A SAED pattern confirmed the presence of all four crystalline phases within individual nanoparticles, in agreement with XRD. Fig. 4c and d also provide further evidence that the core-shell structure of the parent Al-TiO$_2$ nanoparticles are retained following Fe and S modification, resulting in a uniform (~5 nm thick) shells comprising a mix of alumina, hemite and
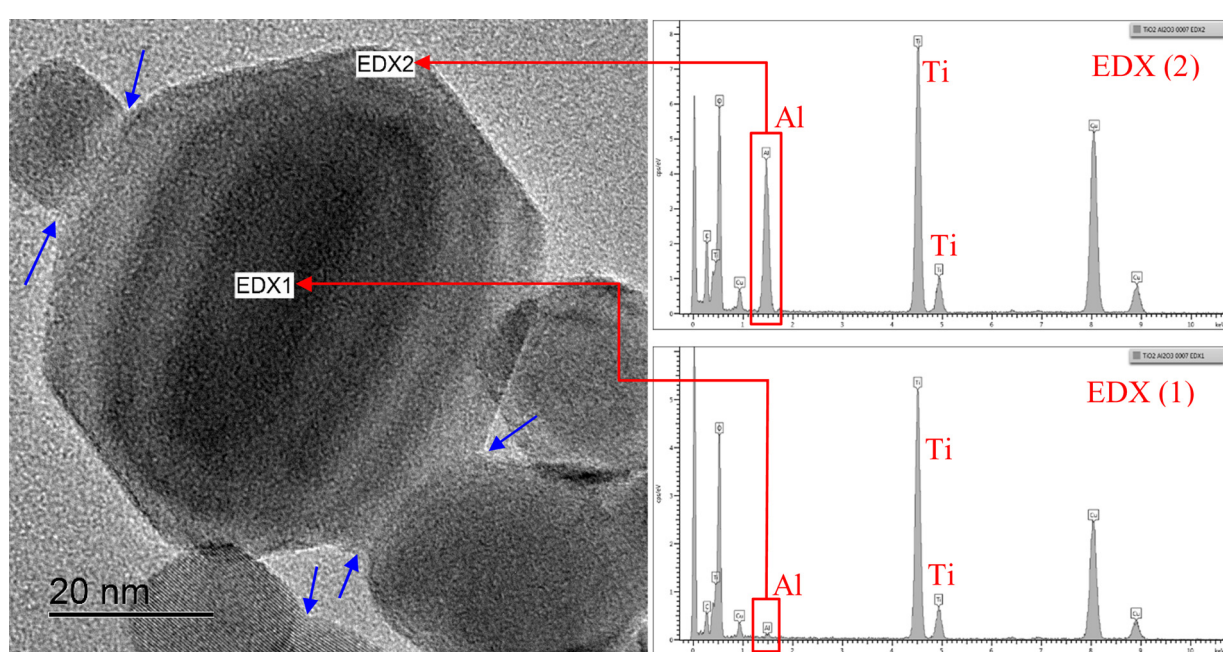

Fig. 2. TEM-EDX spectra for a single particle shows the coating of alumina on the TiO$_2$ NPs. The blue arrows represent the oriented attachment of nanoparticles. (For interpretation of the references to color in this figure legend, the reader is referred to the web version of this article).
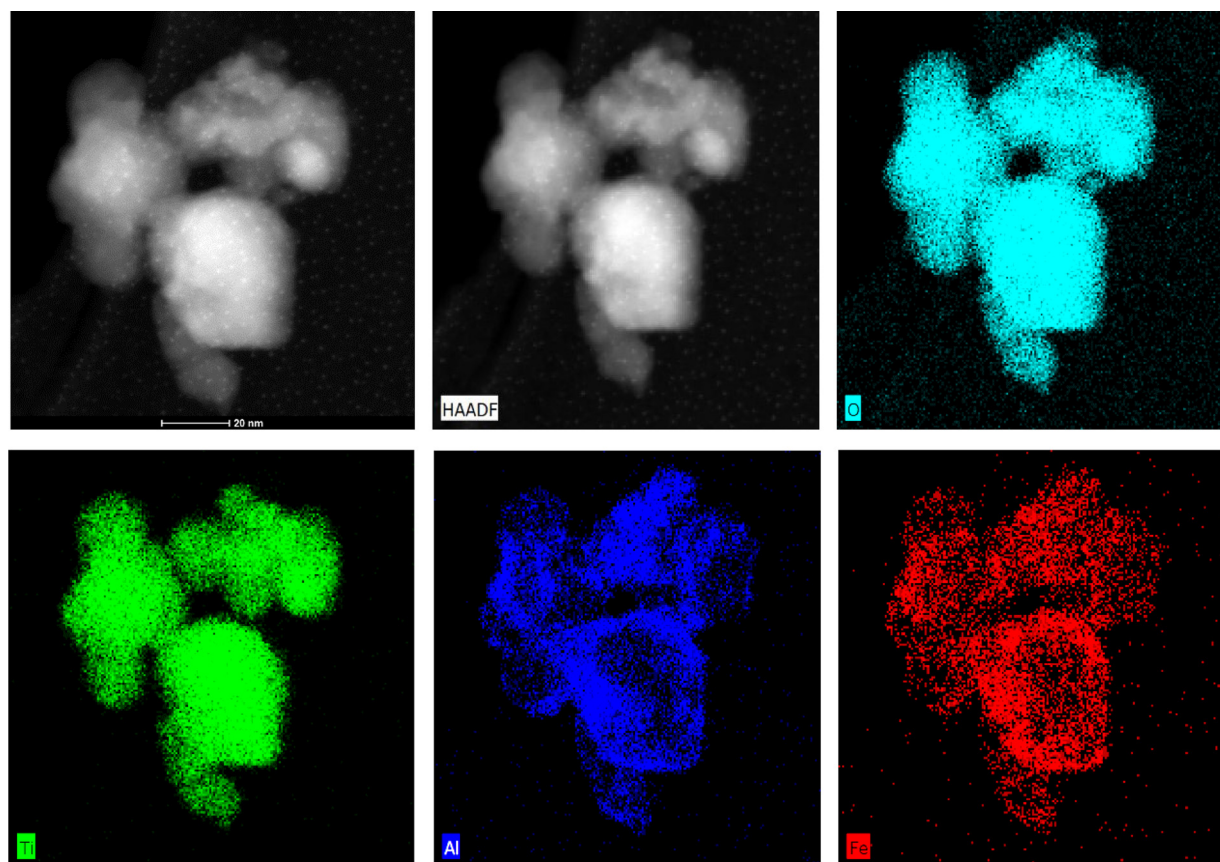
Fig. 3. (clockwise from top left) Dark-field HAADF-STEM, and EDS elemental maps of O, Ti, Al, and Fe highlighting uniform distribution of each component in Fe-Al-TiO$_2$ catalyst.

millosevichite encapsulating anatase and rutile cores.

EDS confirms the presence of O, S, Fe, Al and Ti (Figs. S8 and 9 and Table 3) in the SO$_4$/Fe-Al-TiO$_2$ with S uniformly distributed across the material (Fig. S9).

3.1.3. Surface functionality

The nature of surface sulphoxy species arising from sulfonation was explored by attenuated total reflection (ATR)-FTIR (Fig. 5). Comparison with the parent Fe-Al-TiO$_2$ spectrum reveals that sulfonation results in the appearance of new bands characteristic of sulphate groups, with strong peaks at 980, 1065 and 1138 cm^{-1} assigned to S−O stretches of sulfated metal oxides [19,53–55], and peaks at 1430 and 1469 cm^{-1} attributed to S=O asymmetric and symmetric sulfate stretches respectively. These features are consistent with polynuclear sulphates S$_2$O$_7^{2-}$ or S$_3$O$_{10}^{2-}$ [56], presumably arising from the chlorosulfonic acid dimerization (Fig. S10) prior to surface sulfation. The bands in the region of ∼550 to 780 cm^{-1} in Fe-Al-TiO$_2$ and SO$_4$/Fe-Al-TiO$_2$ likely arise from M−O−M bridging stretches [30,57], and the broad band between 3050–3800 cm^{-1} to surface surface hydroxyls [20,39,55,58] whose presence has been reported to enhance catalytic activity [59]. FTIR thus confirms successful sulfation of Fe-Al-TiO$_2$ particles.

3.1.4. Textural properties

Nitrogen adsorption/desorption isotherms and corresponding pore size and pore volume distributions are shown in Fig. 6 for the parent TiO$_2$ NPs, and for the functionalised Al-TiO$_2$, Fe-Al-TiO$_2$ and SO$_4$/Fe-Al-TiO$_2$ materials. Except for the Fe-Al-TiO$_2$ sample, the materials all exhibited type II adsorption-desorption isotherms characteristic of macroporous materials (or non-porous materials possessing large interparticle voids). The BET surface areas spanned 49–78 m^2 g^{-1} (Table S1) similar to that of the parent titania nanoparticles. All materials

exhibited a single hysteresis loop with that for Fe-Al-TiO$_2$ sample of type II while those of the other materials were of type I [60]. The increase mesoporosity of Fe-Al-TiO$_2$ suggests that iron functionalisation of the alumina-coated titania NPs creates a highly porous second shell, and/or mesoporous interparticle voids between discrete hematite particles and the Al-TiO$_2$ nanoparticles.

3.1.5. Thermal stability

The TGA profiles of all samples (Fig. 7) showed only a small weight loss between room temperature and 150 °C due to physisorbed water [18]. No significant further weight losses were observed for any of the samples except for SO$_4$/Fe-Al-TiO$_2$ which lost approximately 15% of the initial total mass above 633 °C due to decomposition of sulphate groups, indicating excellent thermal stability (other sulphated metal oxides are often reported to decompose > 430 °C [18,56]).

3.1.6. Surface acidity

DRIFTS of pyridine titrated materials was employed to quantify their Brønsted/Lewis acid character (Fig. S11). DRIFT spectra of the samples suggested that all non-sulfonated samples possess a mixture of Lewis and Brønsted acid sites but SO$_4$/Fe-Al-TiO$_2$ catalyst is purely Brønsted acidic as shown in Fig. S11. The shifting of the stretching frequencies of the sulphate groups vibration from Al-TiO$_2$ and Fe-Al-TiO$_2$ and SO$_4$/Fe-Al-TiO$_2$ indicates stronger interaction between the surface sulphur complex and the adsorbed pyridine molecules. This shifting increases the activity of the catalysts [53]. The mode at 1490 cm^{-1} appeared in all catalyst samples indicating the strong coordination of pyridine and pyridinium ions on the Brønsted and Lewis acid sites, respectively [61]. The ratio of Brønsted to Lewis acid (B/L) sites, extracted from the peak areas of 1541 and 1445 cm^{-1}, for all catalysts are summarised in Table 4. Acid loadings were determined
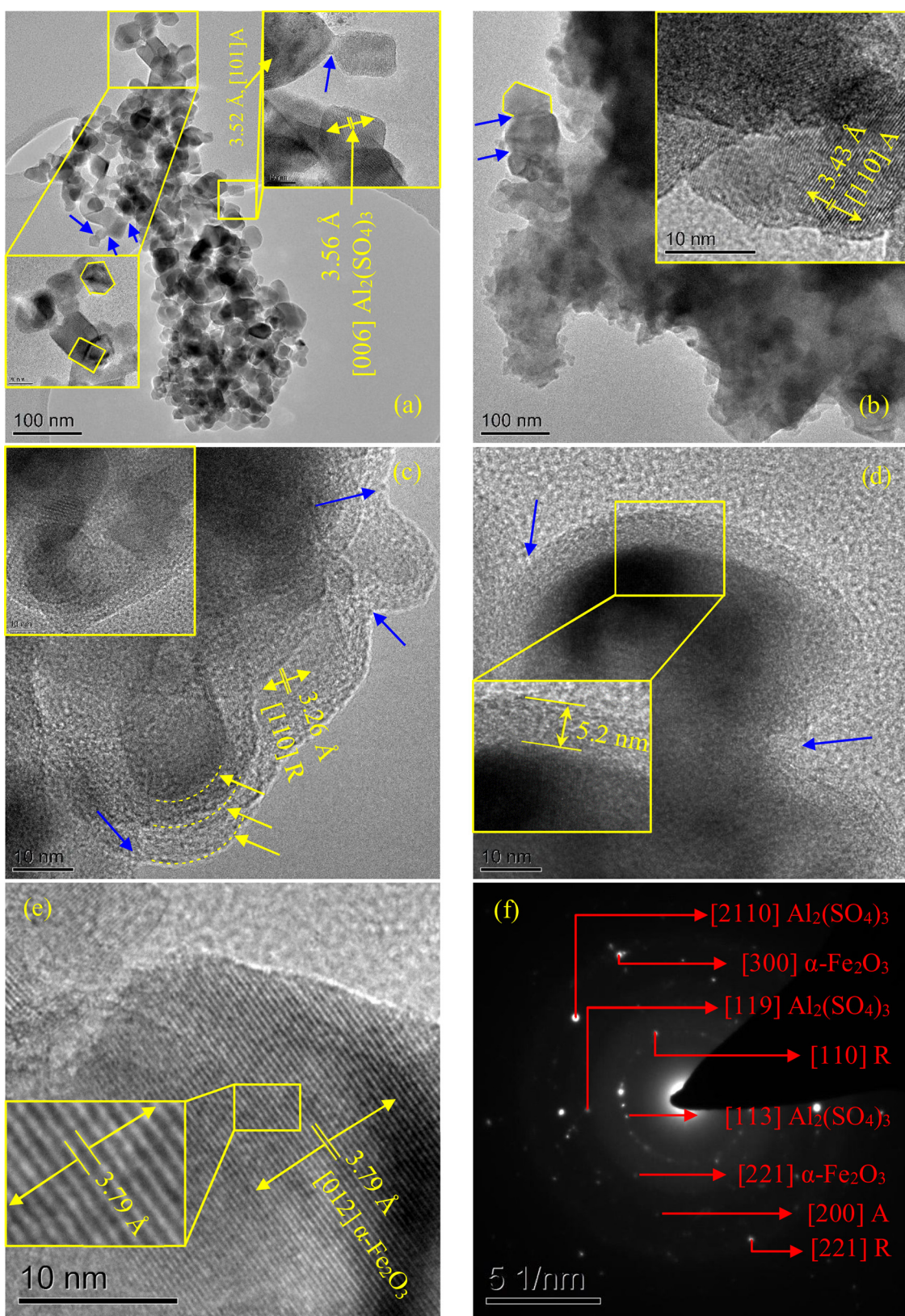
Fig. 4. (a–e) TEM images and (f) SAED of SO$_4$/Fe-Al-TiO$_2$.

from the desorption of reactively-formed propene from *n*-propylamine saturated TiO$_2$ and SO$_4$/Fe-Al-TiO$_2$ samples (Fig. 8) and shown in Table 4. Sulfation dramatically increased the acid loading relative the parent titania NPs as well as some of this acid loading coming from the acid sites formed by iron oxide or alumina layers [20]. In addition to

acting as the catalyst support (nanoparticle core) TiO$_2$ may also introduce some Lewis acidity to complementing the Brønsted acidity of surface sulfate groups.

Table 3
Elemental analysis of $SO_4/Fe-Al-TiO_2$ by EDS.

| Element	O	Al	S	Ti	Fe
Weight%	42.2	14.2	7.6	15.0	21.0
Atomic%	64.0	13.3	5.1	8.0	9.6
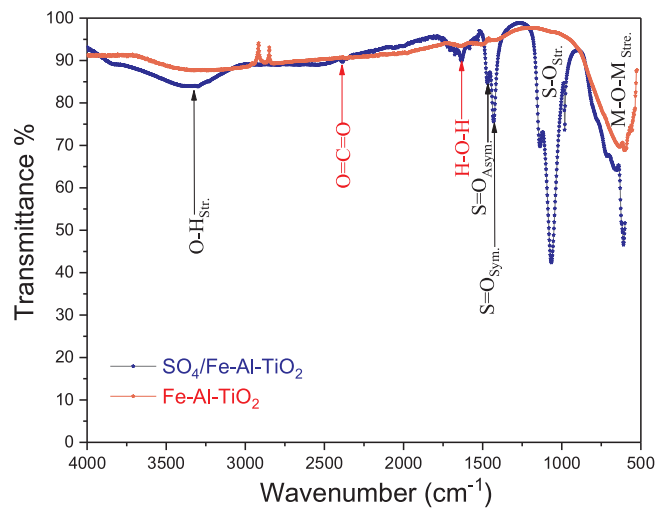
**Fig. 5.** FTIR spectra of $Fe-Al-TiO_2$ and $SO_4/Fe-Al-TiO_2$.
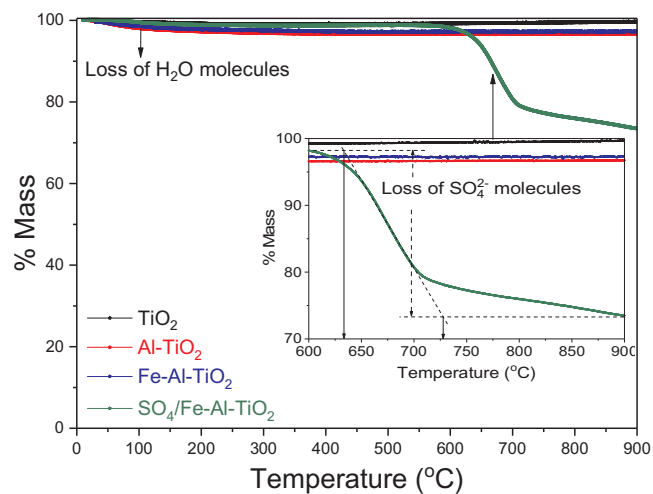
Fig. 7. TGA profiles for TiO_2 NPs, $Al-TiO_2$, $Fe-Al-TiO_2$ and $SO_4/Fe-Al-TiO_2$.

3.1.7. Magnetic properties

The magnetisation curve for $SO_4/Fe-Al-TiO_2$ was measured at room temperature between 2 and −2 T. The resulting hysteresis loop is shown in Fig. 9. The magnetic field (M) versus applied magnetic field (H) curve indicates a saturation magnetisation value of the sample at ~10 emu/g. The saturation magnetisation value for pure iron oxide (Fe_2O_3 and Fe_3O_4) is higher than $SO_4/Fe-Al-TiO_2$. However, $SO_4/Fe-Al-TiO_2$ still exhibited super paramagnetic behaviour (M_r = 0.65 emu/g
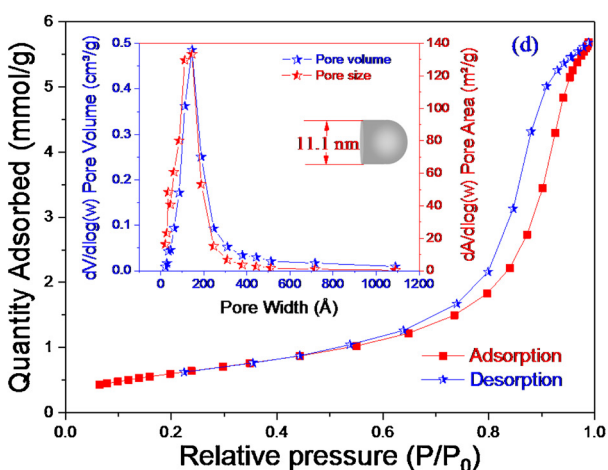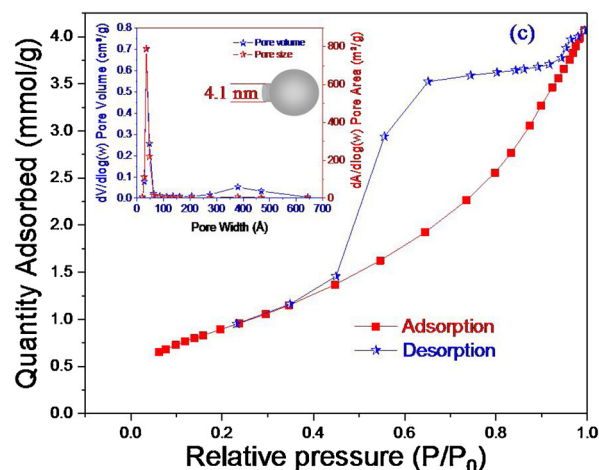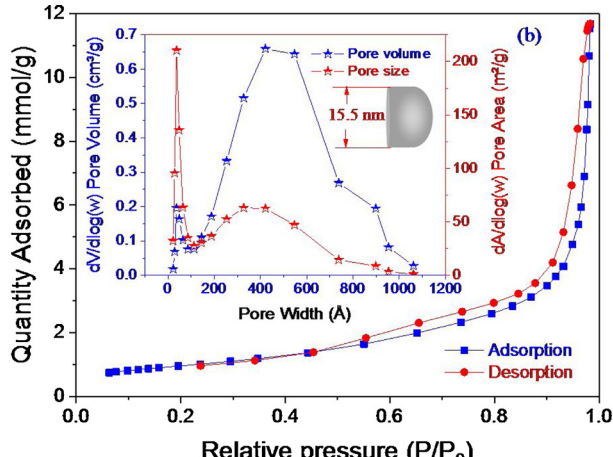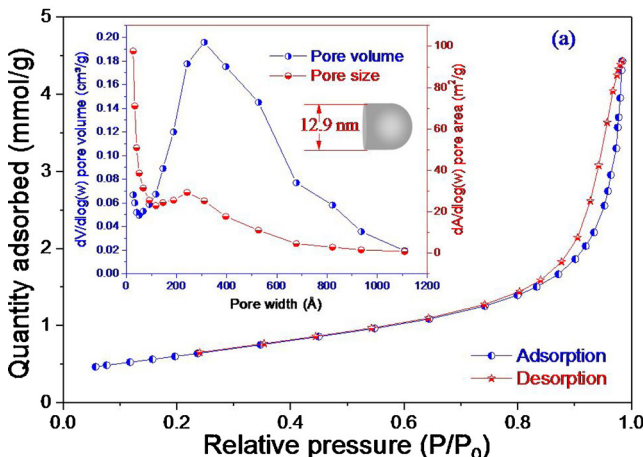
**Fig. 6.** N_2 adsorption-desorption isotherms and total pore volumes with mean pore sizes (inset) for catalysts (a) TiO_2, (b) $Al-TiO_2$, (c) $Fe-Al-TiO_2$ and (d) $SO_4/Fe-Al-TiO_2$.

Table 4
Acidic properties of the synthesised materials.

Materials	Brønsted:Lewis ratio	Acid loading/mmol g^{-1}
TiO$_2$	0.05	0.28
Al-TiO$_2$	0.33	–
Fe-Al-TiO$_2$	0.13	–
SO$_4$/Fe-Al-TiO$_2$	3.58	1.18

and H$_c$ = 0.0024 T as seen in the inset for Fig. 9) which has been shown sufficient to effect separation of magnetic catalysts from reaction media [45].

3.2. Catalytic performance

The SO$_4$/Fe-Al-TiO$_2$ material was subsequently evaluated for the simultaneous esterification and transesterification of WCO to produce biodiesel. Optimum reaction conditions were explored through examining the impact of methanol:WCO stoichiometry, temperature, and catalyst loading on FAME yield. Fig. 10a shows the time dependence of FAME production for 1.5 wt% SO$_4$/Fe-Al-TiO$_2$, a methanol:WCO molar ratio of 9:1 and reaction temperature of 75 °C (these initial conditions chosen from our previous studies on Ti(SO$_4$)O catalysts [5]). FAME yield increased linearly with time before reaching a plateau at 83% after 2.5 h. The effect of catalyst mass was subsequently explored (Fig. 10b) at a methanol:WCO molar ratio of 9:1 after 2.5 h reaction at 75 °C, with increases between 0.5–1.5 wt% resulting in a linear increase in FAME yield to a maximum of 91%; additional catalyst loadings had negligible impact. This observation shows that esterification/transesterification were reaction-rate limited for loadings ≤1.5 wt% and that higher loadings are therefore undesirable. Since esterification and transesterification are both reversible, excess methanol is employed to shift the equilibrium reaction towards FAME, with methanol:oil molar ratios between 3–60:1 commonly employed; higher methanol concentrations promote oil solubility and hence FAME yields [62–64].

Fig. 10c shows the effect of methanol:WCO ratio with 3 wt% catalyst after 2.5 h reaction at 75 °C. FAME yield was directly proportional to the methanol:WCO ratio between 1:1–10:1, with a limiting value of 92% again attained. Finally, the impact of reaction temperature was assessed between 25–90 °C (Fig. 10d) for 3 wt% catalyst and a 10:1 methanol:oil molar ratio after 2.5 h reaction. FAME yield increased continuously for temperatures < 75 °C, reaching a limiting value of 95%, probably reflecting both increased reactant activation and higher oil miscibility [20]. Higher temperatures had negligible impact on FAME production indicating that the reaction had reached equilibrium.

The sensitivity of SO$_4$/Fe-Al-TiO$_2$ to FFA within bio-oil feedstocks

was also explored by evaluating catalytic performance in the transesterification of a virgin corn oil feedstock deliberately spiked with between 0.5–20 wt% oleic acid (as a model FFA) using the optimum reaction conditions determined above (Fig. 11a): 3 wt% catalyst loading, 10:1 methanol:oil, and 90 °C after 2.5 h reaction). Surprisingly, the FAME yield remained at 95% independent of the FFA content of the oil feedstock, indicating a robust catalyst. Catalyst lifetime was also assessed in 10 consecutive reactions (Fig. 11b) under the same reaction conditions, employing magnetic separation to recover the spent catalyst each time. The spent catalyst was washed repeatedly with a 1:1 vol% methanol:n-hexane mixture to remove any organic residues, and then calcined for 2 h at 250 °C before addition to a fresh reaction mixture. Excellent stability was again evidence by retention of a high (> 90%) FAME yield for 10 recycles. Powder XRD patterns of the spent catalyst after each reaction confirmed retention of the crystalline phases present in the fresh material (Fig. S12).

Table 5 compares the performance of SO$_4$/Fe-Al-TiO$_2$ with some solid acid catalysts from literature, showing that the catalyst synthesized in this study can produce similar amount of FAME (96% FAME) at much milder reaction temperature and shorter time. Although our previously reported Ti(SO$_4$)O catalyst gave an excellent 97% FAME yield from a WCO feedstock under similar reaction conditions (albeit a lower temperature and catalyst loading), this was less robust than the present SO$_4$/Fe-Al-TiO$_2$ catalyst, deactivating after 10 recycles due to sulfate leaching. It is also important to note that Ti(SO$_4$)O was only effective for WCO containing ≤6 wt% FFA, versus 20 wt% for SO$_4$/Fe-Al-TiO$_2$. Al and Fe within SO$_4$/Fe-Al-TiO$_2$ may inhibit sulfate leaching [65]. In addition to this, water by-product from the esterification of oleic acid (as a model FFA) had no significant impact on the deactivation or poisoning of active sites in the SO$_4$/Fe-Al-TiO$_2$ catalyst, and SO$_4$/Fe-Al-TiO$_2$ is readily separated from the reaction mixture by an external magnetic field.

3.3. Biodiesel characterisation

The biodiesel derived from the esterification and transesterification of WCO over SO$_4$/Fe-Al-TiO$_2$ was analysed and characterised according to ASTM and/or EN standards and the results summarized in Tables S2 and S3. The principal FAME components in Table S2 were methyl palmitate, methyl oleate and methyl linoleate. The physical characteristics of the biodiesel properties conformed with ASTM and EU standards, with a cloud point of −11.3 °C (Fig. S13). Decomposition/combustion of the synthetic biodiesel occurred > 144 °C and was complete by 226 °C (Fig. S14).
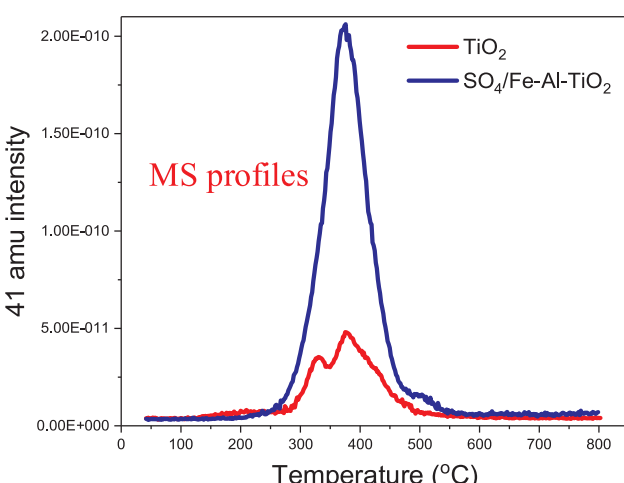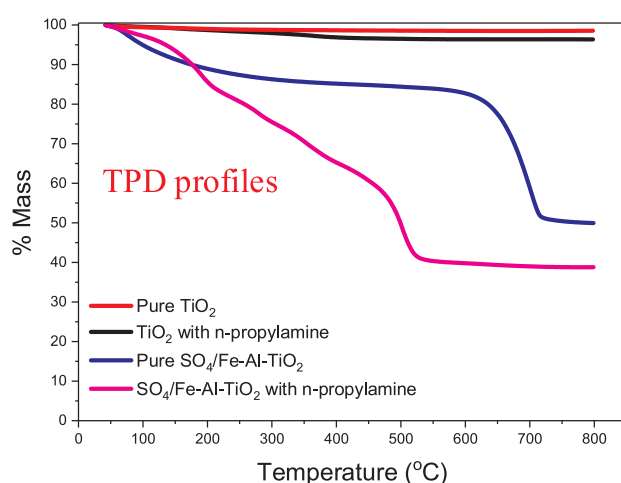

Fig. 8. (left) Thermograms, and (right) mass spectra for TiO$_2$ NPs and SO$_4$/Fe-Al-TiO$_2$ of pure and saturated with n-propylamine.
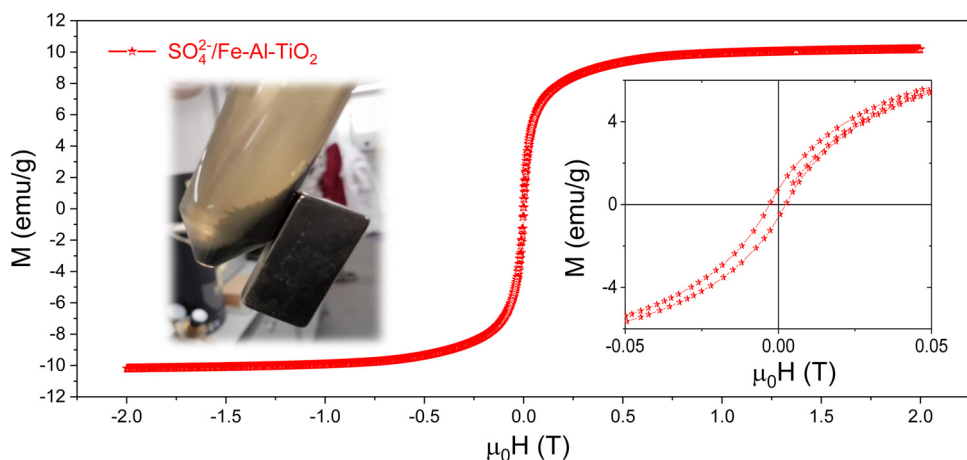
Fig. 9. Magnetisation hysteresis loop of SO_4/Fe-Al-TiO$_2$ at room temperature (left inset). photograph demonstrating magnetic separation of material from solution (right inset).
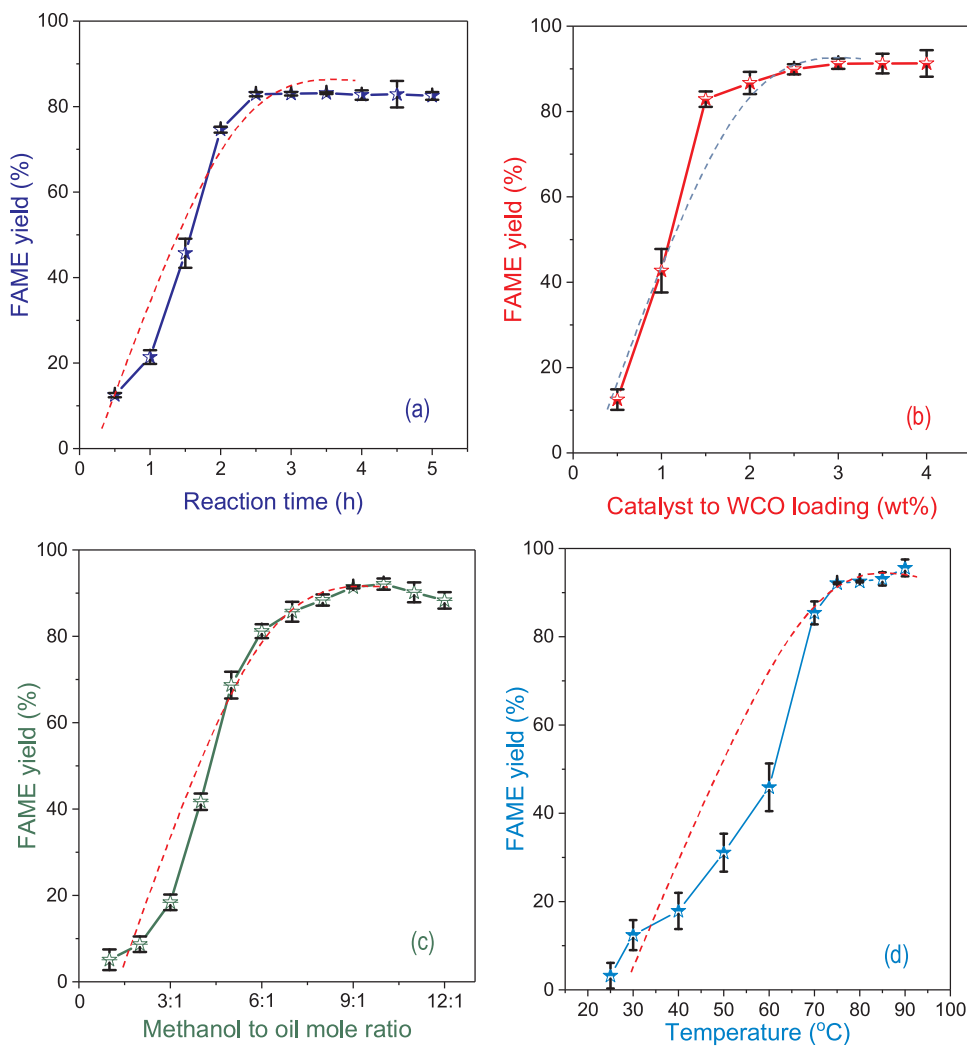

Fig. 10. Effects of (a) reaction time, (b) catalyst loading, (c) methanol to WCO molar ratio, and (d) reaction temperature 1on the FAME yield using synthesized SO_4/Fe-Al-TiO$_2$ catalyst.

4. Conclusions

A super paramagnetic solid acid catalyst comprising SO_4/Fe-Al-TiO$_2$ was prepared by the stepwise functionalise of titania NPs. Extensive characterisation of the catalyst bulk and surface properties revealed it possessed a high acid loading and Brønsted acid character arising from surface sulfate and persulfate species generated by chlorosulfonic acid functionalisation, and strong magnetic character arising from hematite nanoparticle. SO_4/Fe-Al-TiO$_2$ exhibited promising activity for the (trans)esterification of WCO to biodiesel. Under optimum conditions of
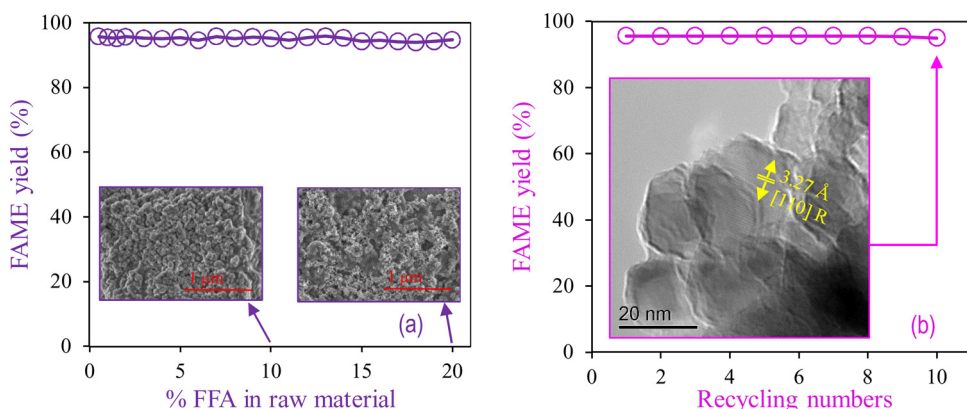
Fig. 11. Effect of (a) oleic acid content and (b) recycling of SO_4/Fe-Al-TiO_2 catalyst on the FAME yield. The inset TEM result for the recovered spent catalyst from WCO transesterification process after run 10 shows a clear [110] facets for the rutile TiO_2 NPs (ICDD: 01-076-9000).

Table 5
Comparison of sulfated metal oxide catalysts for biodiesel production from WCO.

	This work	Gardy et al. [5]	Alhassan et al. [31]	Wang et al. [66]
Feedstock	WCO	WCO	WCO	WCO
Methanol:oil ratio	10:1	9:1	20:1	10:1
Catalyst	SO_4/Fe-Al-TiO_2	Ti(SO_4)O	Fe_2O_3-MnO-SO_4/ZrO_2	SO_4^{2-}/TiO_2/La^{+3}
Catalyst loading/wt %	3	1.5	3	5
Reaction time/h	2.5	3	6	1
Particle size/nm	47	25	–	–
Surface area/ $m^2 g^{-1}$	51	45	72	229
Temperature/°C	90	75	180	110
FAME yield/%	96	97	96	> 90
Recycles	10 (94 %)	10 (73 %)	7 (94 %)	5 (90%)

3 wt% catalyst, a 10:1 molar ratio of methanol:WCO molar and 90 °C, a 95.6% FAME yield was attained after 2.5 h reaction. The SO_4/Fe-Al-TiO_2 catalyst exhibited excellent stability and recyclability employing magnetic separation and thermal regeneration, maintaining a high performance for virgin corn oil transesterification even in the presence of up to 20 wt% oleic acid, and for over 10 consecutive reactions cycles with WCO.

Conflicts of interest

The authors declare no conflict of interest.

Acknowledgments

Appendix A. Supplementary data

Supplementary material related to this article can be found, in the online version, at doi:https://doi.org/10.1016/j.apcatb.2018.04.046.

References

[1] N. Armaroli, V. Balzani, The future of energy supply: challenges and opportunities, Angew. Chem. Int. Ed. 46 (1–2) (2007) 52–66.

[2] M. Rehan, J. Gardy, A. Demirbas, U. Rashid, W. Budzianowski, D. Pant, A. Nizami, Waste to biodiesel: a preliminary assessment for Saudi Arabia, Bioresour. Technol. 250 (2018) 17–25.

[3] J.-P. Dacquin, A.F. Lee, C. Pirez, K. Wilson, Pore-expanded SBA-15 sulfonic acid silicas for biodiesel synthesis, Chem. Commun. 48 (2) (2012) 212–214.

[4] J. Gardy, A. Hassanpour, X. Lai, M. Rehan, The influence of blending process on the quality of rapeseed oil-used cooking oil biodiesels, Int. Sci. J. Environ. Sci. 3 (2014) 233–240.

[5] J. Gardy, A. Hassanpour, X. Lai, M.H. Ahmed, Synthesis of Ti(SO_4)O solid acid nano-catalyst and its application for biodiesel production from used cooking oil, Appl. Catal. A 527 (2016) 81–95.

[6] K.A. Salam, S.B. Velasquez-Orta, A.P. Harvey, A sustainable integrated in situ transesterification of microalgae for biodiesel production and associated co-products- a review, Renew. Sustain. Energy Rev. 65 (2016) 1179–1198.

[7] V.G. Gude, G.E. Grant, Biodiesel from waste cooking oils via direct sonication, Appl. Energy 109 (2013) 135–144.

[8] S. Wahidin, A. Idris, S.R.M. Shaleh, Rapid biodiesel production using wet microalgae via microwave irradiation, Energy Convers. Manage. 84 (2014) 227–233.

[9] S.H. Shuit, K.T. Lee, A.H. Kamaruddin, S. Yusup, Reactive extraction and in situ esterification of Jatropha curcas L. seeds for the production of biodiesel, Fuel 89 (2) (2010) 527–530.

[10] J. Jitputti, B. Kitiyanan, P. Rangsunvigit, K. Bunyakiat, L. Attanatho, P. Jenvanitpanjakul, Transesterification of crude palm kernel oil and crude coconut oil by different solid catalysts, Chem. Eng. J. 116 (1) (2006) 61–66.

[11] D. Rattanaphra, A. Harvey, P. Srinophakun, Simultaneous conversion of triglyceride/free fatty acid mixtures into biodiesel using sulfated zirconia, Top. Catal. 53 (11–12) (2010) 773–782.

[12] J. Gardy, Biodiesel production from used cooking oil using novel solid acid catalysts, School of Chemical and Process Engineering, University of Leeds: United Kingdom, Leeds, 2017 White Rose etheses.

[13] A.F. Lee, J.A. Bennett, J.C. Manayil, K. Wilson, Heterogeneous catalysis for sustainable biodiesel production via esterification and transesterification, Chem. Soc. Rev. 43 (22) (2014) 7887–7916.

[14] J.C. Manayil, C.V. Inocencio, A.F. Lee, K. Wilson, Mesoporous sulfonic acid silicas for pyrolysis bio-oil upgrading via acetic acid esterification, Green Chem. 18 (5) (2016) 1387–1394.

[15] A. Guldhe, P. Singh, F.A. Ansari, B. Singh, F. Bux, Biodiesel synthesis from microalgal lipids using tungstated zirconia as a heterogeneous acid catalyst and its comparison with homogeneous acid and enzyme catalysts, Fuel 187 (2017) 180–188.

[16] J. Gardy, A. Hassanpour, X. Lai, M.H. Ahmed, M. Rehan, Biodiesel production from used cooking oil using a novel surface functionalised TiO_2 nano-catalyst, Appl. Catal. B: Environ. 207 (2017) 297–310.

[17] S. Furuta, H. Matsuhashi, K. Arata, Biodiesel fuel production with solid amorphous-zirconia catalysis in fixed bed reactor, Biomass Bioenergy 30 (10) (2006) 870–873.

[18] J. Wang, P. Yang, M. Fan, W. Yu, X. Jing, M. Zhang, X. Duan, Preparation and characterization of novel magnetic ZrO_2/TiO_2/Fe_3O_4 solid superacid, Mater. Lett. 61 (11) (2007) 2235–2238.

[19] R.M. De Almeida, L.K. Noda, N.S. Gonçalves, S.M. Meneghetti, M.R. Meneghetti, Transesterification reaction of vegetable oils, using superacid sulfated TiO_2–base catalysts, Appl. Catal. A 347 (1) (2008) 100–105.

[20] M.K. Lam, K.T. Lee, A.R. Mohamed, Sulfated tin oxide as solid superacid catalyst for transesterification of waste cooking oil: an optimization study, Appl. Catal. B: Environ. 93 (1) (2009) 134–139.

[21] A. Jenie, D.S. Kusuma, A. Kristiani, J.A. Laksmono, S. Tursiloadi, Preparation and characterization of sulfated titania catalysts for the isomerisation of citronellal, Int. J. Basic Appl. Sci. 10 (06) (2010) 5–10.

[22] D. Guan, M. Fan, J. Wang, Y. Zhang, Q. Liu, X. Jing, Synthesis and properties of magnetic solid superacid: SO_4^{2-}/ZrO_2–B_2O_3–Fe_3O_4, Mater. Chem. Phys. 122 (1) (2010) 278–283.

[23] Z. Wen, X. Yu, S.-T. Tu, J. Yan, E. Dahlquist, Biodiesel production from waste cooking oil catalyzed by TiO_2–MgO mixed oxides, Bioresour. Technol. 101 (24) (2010) 9570–9576.

[24] Y. Li, X.-D. Zhang, L. Sun, M. Xu, W.-G. Zhou, X.-H. Liang, Solid superacid catalyzed

fatty acid methyl esters production from acid oil, Appl. Energy 87 (7) (2010) 2369–2373.

[25] P. Valle-Vigón, M. Sevilla, A.B. Fuertes, Sulfonated mesoporous silica–carbon composites and their use as solid acid catalysts, Appl. Surf. Sci. 261 (2012) 574–583.

[26] J. Shen, Y. Zhu, X. Yang, C. Li, Magnetic composite microspheres with exposed {001} faceted TiO_2 shells: a highly active and selective visible-light photocatalyst, J. Mater. Chem. 22 (26) (2012) 13341–13347.

[27] R. Madhuvilakku, S. Piraman, Biodiesel synthesis by TiO_2–ZnO mixed oxide na-nocatalyst catalyzed palm oil transesterification process, Bioresour. Technol. 150 (2013) 55–59.

[28] S. Qin, W. Cai, X. Tang, L. Yang, Sensitively monitoring photodegradation process of organic dye molecules by surface-enhanced Raman spectroscopy based on Fe_3O_4@SiO_2@TiO_2@Ag particle, Analyst 139 (21) (2014) 5509–5515.

[29] A. Osatiashtiani, A.F. Lee, D.R. Brown, J.A. Melero, G. Morales, K. Wilson, Bifunctional SO_4^{2-}/$ZrO2$ catalysts for 5-hydroxymethylfufural (5-HMF) produc-tion from glucose, Catal. Sci. Technol. 4 (2) (2014) 333–342.

[30] C. Li, J. Tan, X. Fan, B. Zhang, H. Zhang, Q. Zhang, Magnetically separable one dimensional Fe_3O_4/P(MAA-DVB)/TiO_2 nanochains: preparation, characterization and photocatalytic activity, Ceram. Int. 41 (3) (2015) 3860–3868.

[31] F.H. Alhassan, U. Rashid, Y. Taufiq-Yap, Synthesis of waste cooking oil-based bio-diesel via effectual recyclable bi-functional Fe_2O_3-MnO-SO_4^{2-}/ZrO_2 nanoparticle solid catalyst, Fuel 142 (2015) 38–45.

[32] R.Z. Raia, L.S. da Silva, S.M.P. Marcucci, P.A. Arroyo, Biodiesel production from Jatropha curcas L. oil by simultaneous esterification and transesterification using sulphated zirconia, Catal. Today (2016).

[33] A. Osatiashtiani, L.J. Durndell, J.C. Manayil, A.F. Lee, K. Wilson, Influence of alkyl chain length on sulfated zirconia catalysed batch and continuous esterification of carboxylic acids by light alcohols, Green Chem. 18 (20) (2016) 5529–5535.

[34] L.K. Noda, R.M. de Almeida, N.S. Gonçalves, L.F.D. Probst, O. Sala, TiO_2 with a high sulfate content—thermogravimetric analysis, determination of acid sites by infrared spectroscopy and catalytic activity, Catal. Today 85 (1) (2003) 69–74.

[35] H. Zhang, H. Yu, A. Zheng, S. Li, W. Shen, F. Deng, Reactivity enhancement of 2-Propanol photocatalysis on SO_4^{2-}/TiO_2: insights from solid-state NMR spectro-scopy, Environ. Sci. Technol. 42 (14) (2008) 5316–5321.

[36] Z. Li, R. Wnetrzak, W. Kwapinski, J.J. Leahy, Synthesis and characterization of sulfated TiO_2 nanorods and ZrO_2/TiO_2 nanocomposites for the esterification of biobased organic acid, ACS Appl. Mater. Interfaces 4 (9) (2012) 4499–4505.

[37] Y.-X. Jiang, X.-M. Chen, Y.-F. Mo, Z.-F. Tong, Preparation and properties of Al-PILC supported SO_4^{2-}/$TiO2$ superacid catalyst, J. Mol. Catal. A Chem. 213 (2) (2004) 231–234.

[38] D.-m. Lai, L. Deng, Q.-x. Guo, Y. Fu, Hydrolysis of biomass by magnetic solid acid, Energy Environ. Sci. 4 (9) (2011) 3552–3557.

[39] L. Wu, Y. Zhou, W. Nie, L. Song, P. Chen, Synthesis of highly monodispersed teardrop-shaped core–shell SiO_2/TiO_2 nanoparticles and their photocatalytic ac-tivities, Appl. Surf. Sci. 351 (2015) 320–326.

[40] M.J. Jacinto, O.H. Santos, R.F. Jardim, R. Landers, L.M. Rossi, Preparation of re-coverable Ru catalysts for liquid-phase oxidation and hydrogenation reactions, Appl. Catal. A 360 (2) (2009) 177–182.

[41] A.H. Lu, E.L. Salabas, F. Schüth, Magnetic nanoparticles: synthesis, protection, functionalization, and application, Angew. Chem. Int. Ed. 46 (8) (2007) 1222–1244.

[42] S. Sobhani, Z.P. Parizi, N. Razavi, Nano n-propylsulfonated γ-Fe_2O_3 as magnetically recyclable heterogeneous catalyst for the efficient synthesis of β-phosphonomalo-nates, Appl. Catal. A 409 (2011) 162–166.

[43] S. Tang, L. Wang, Y. Zhang, S. Li, S. Tian, B. Wang, Study on preparation of Ca/Al/$Fe3O4$ magnetic composite solid catalyst and its application in biodiesel transes-terification, Fuel Process. Technol. 95 (2012) 84–89.

[44] T. Xin, M. Ma, H. Zhang, J. Gu, S. Wang, M. Liu, Q. Zhang, A facile approach for the synthesis of magnetic separable Fe_3O_4@ TiO_2, core–shell nanocomposites as highly recyclable photocatalysts, Appl. Surf. Sci. 288 (2014) 51–59.

[45] H. Moghanian, A. Mobinikhaledi, A. Blackman, E. Sarough-Farahani, Sulfanilic acid-functionalized silica-coated magnetite nanoparticles as an efficient, reusable and magnetically separable catalyst for the solvent-free synthesis of 1-amido-and 1-aminoalkyl-2-naphthols, RSC Adv. 4 (54) (2014) 28176–28185.

[46] M. Zabeti, W.M.A.W. Daud, M.K. Aroua, Activity of solid catalysts for biodiesel production: a review, Fuel Process. Technol. 90 (6) (2009) 770–777.

[47] S. Anuradha, K. Raj, V. Vijayaraghavan, B. Viswanathan, Sulphated Fe_2O_3-TiO_2 catalysed transesterification of soybean oil to biodiesel, Indian J. Chem. 53A (2014) 1493–1499.

[48] T. Bhongsuwan, D. Bhongsuwan, N. Chomchoey, L. Boonchuay, Effect of calcination temperature in production of magnetic nanoparticles for arsenic adsorption, Mater. Chem. Phys. 110 (2-3) (2008) 426–433.

[49] R. Massart, Preparation of aqueous magnetic liquids in alkaline and acidic media, IEEE Trans. Magn. 17 (2) (1981) 1247–1248.

[50] D.A. Hanaor, C.C. Sorrell, Review of the anatase to rutile phase transformation, J. Mater. Sci. 46 (4) (2011) 855–874.

[51] ASTM-D974, Standard Test Method for Acid and Base Number by Colour-Indicator Titration, (2012), pp. 1–7.

[52] EN-14104, Fat and Oil Derivatives-Fatty Acid Methyl Esters (FAME): Determination of Acid Value, (2003).

[53] T. Jin, T. Yamaguchi, K. Tanabe, Mechanism of acidity generation on sulfur-pro-moted metal oxides, J. Phys. Chem. 90 (20) (1986) 4794–4796.

[54] L.K. Noda, R.M. de Almeida, L.F.D. Probst, N.S. Gonçalves, Characterization of sulfated TiO_2 prepared by the sol–gel method and its catalytic activity in the n-hexane isomerization reaction, J. Mol. Catal. A Chem. 225 (1) (2005) 39–46.

[55] J. Ropero-Vega, A. Aldana-Pérez, R. Gómez, M. Niño-Gómez, Sulfated titania [TiO_2/SO_4 $^{2-}$]: a very active solid acid catalyst for the esterification of free fatty acids with ethanol, Appl. Catal. A 379 (1) (2010) 24–29.

[56] Y.R. Smith, K.J.A. Raj, V.R. Subramanian, B. Viswanathan, Sulfated Fe_2O_3–TiO_2 synthesized from ilmenite ore: a visible light active photocatalyst, Colloids Surf. A: Physicochem. Eng. Aspects 367 (1) (2010) 140–147.

[57] H. Naeimi, Z.S. Nazifi, A highly efficient nano-Fe_3O_4 encapsulated-silica particles bearing sulfonic acid groups as a solid acid catalyst for synthesis of 1, 8-dioxo-octahydroxanthene derivatives, J. Nanopart. Res. 15 (11) (2013) 2026.

[58] M. Jafar Tafreshi, Z. Masoomi Khanghah, Infrared spectroscopy studies on sol-gel prepared alumina powders, Mater. Sci. 21 (1) (2015) 28–31.

[59] Y.-M. Park, D.-W. Lee, D.-K. Kim, J.-S. Lee, K.-Y. Lee, The heterogeneous catalyst system for the continuous conversion of free fatty acids in used vegetable oils for the production of biodiesel, Catal. Today 131 (1) (2008) 238–243.

[60] P. Klobes, K. Meyer, R.G. Munro, Porosity and Specific Surface Area Measurements for Solid Materials. Vol. Special Publication 960-17, US Department of Commerce, Technology Administration, National Institute of Standards and Technology, US, Washington, 2006, p. 88.

[61] M. Tao, L. Xue, Z. Sun, S. Wang, X. Wang, J. Shi, Tailoring the synergistic Brønsted-Lewis acidic effects in heteropolyacid catalysts: applied in esterification and transesterification reactions, Sci. Rep. (2015) 5.

[62] E. Leclercq, A. Finiels, C. Moreau, Transesterification of rapeseed oil in the presence of basic zeolites and related solid catalysts, J. Am. Oil Chem. Soc. 78 (11) (2001) 1161–1165.

[63] S. Furuta, H. Matsuhashi, K. Arata, Biodiesel fuel production with solid superacid catalysis in fixed bed reactor under atmospheric pressure, Catal. Commun. 5 (12) (2004) 721–723.

[64] Q. Shu, J. Gao, Z. Nawaz, Y. Liao, D. Wang, J. Wang, Synthesis of biodiesel from waste vegetable oil with large amounts of free fatty acids using a carbon-based solid acid catalyst, Appl. Energy 87 (8) (2010) 2589–2596.

[65] S. Anuradha, K. Raj, V. Vijayaraghavan, B. Viswanathan, Sulphated Fe_2O_3-TiO_2 catalysed transesterification of soybean oil to biodiesel, Indian J. Chem. 53A (2014) 1493–1499.

[66] K. Wang, J. Jiang, Z. Si, X. Liang, Biodiesel production from waste cooking oil catalyzed by solid acid SO_4^{2-}/TiO_2/La^{3+}, J. Renew. Sustain. Energy 5 (5) (2013) p. 052001.